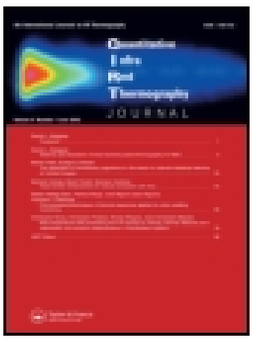

Quantitative InfraRed Thermography Journal

ISSN: 1768-6733 (Print) 2116-7176 (Online) Journal homepage: https://www.tandfonline.com/loi/tqrt20

Comparison of optimisation strategies for the improvement of depth detection capability of Pulse-Compression Thermography

H. Malekmohammadi, S. Laureti, P. Burrascano & M. Ricci

To cite this article: H. Malekmohammadi, S. Laureti, P. Burrascano & M. Ricci (2019): Comparison of optimisation strategies for the improvement of depth detection capability of Pulse-Compression Thermography, Quantitative InfraRed Thermography Journal, DOI: 10.1080/17686733.2019.1603824

To link to this article: https://doi.org/10.1080/17686733.2019.1603824

Published online: 16 May 2019.

QUANTITATIVE INFRARED THERMOGRAPHY JOURNAL
https://doi.org/10.1080/17686733.2019.1603824

Taylor & Francis
Taylor & Francis Group

Comparison of optimisation strategies for the improvement of depth detection capability of Pulse-Compression Thermography

H. Malekmohammadi[a], S. Laureti[a], P. Burrascano[a] and M. Ricci[b]

[a]Department of Engineering, University of Perugia, Terni, TR, Italy; [b]Department of Informatics, Modeling, Electronics and System Engineering, University of Calabria, Rende, CS, Italy

ABSTRACT

In Pulse-Compression Thermography, the impulse response of the Sample Under Test is retrieved pixelwise by applying a proper matched filter on the set of acquired thermal images obtained by stimulating the system with a heat source amplitude – modulated by a proper coded signal. Linear frequency-modulated chirp signals and binary codes are the most employed coded excitations, and to improve the detection capability of the technique, a non-linear frequency-modulated chirp signal can be used to deliver more energy to the sample in a frequency range of interest. In this work, we report the application of an exponential chirp to modulate the heating source and we compare it with a standard linear chirp excitation. To do a fair comparison, various windowing functions have been applied on the matched filters to reduce range side lobes, thus enhancing the retrieved impulse response quality. It is shown that the combined use of an exponential chirp and an appropriate matched filter obtained by exploiting the Reactance Transform window provides a faithful reconstruction of the sample impulse response and an enhanced signal-to-noise ratio with respect to the use of linear chirp. This has been demonstrated on a 3D-printed polymethyl methacrylate (PMMA) sample containing 16 flat-bottom holes of different depths.

ARTICLE HISTORY
Received 3 November 2018
Accepted 4 April 2019

KEYWORDS
Pulse-compression; thermography; windowing; matched filter; 3D-printed PMMA

1. Introduction

Active Thermography (AT) is a non-destructive evaluation technique employed in different research and industrial fields, such as material characterisation [1,2], defect detection [3], cultural heritage diagnostic [4,5] and food inspection [6]. AT always relies on exciting the Sample Under Test (SUT) with either an internal or external heating source to reach the desired thermal contrast [7].

So far, AT has been exploited in two main schemes: Pulsed Thermography (PT) and Lock-in Thermography (LT) [3,8,9]. In PT, a short time duration δ-like heating stimulus is used to excite the SUT within an extended bandwidth. The features of interest are then extracted by analysing pixelwise both the heating and the cooling trends of the acquired impulse response $h(t)$. In LT, the excitation is in a narrow frequency band

CONTACT H. Malekmohammadi hamed.malekmohammadi@unipg.it Department of Engineering, University of Perugia, Strada di Pentima 4, 05100, Terni, Italy

but in wider time span, providing less information but increased signal-to-noise ratio (SNR) with respect to PT.

In recent years, Pulse-Compression Thermography (PuCT) [10–15] has been proposed and developed to overcome the shortcomings and combine the advantages of LT and PT. In PuCT, a broadband-coded heating stimulus is used to heat up the SUT. The main advantage of using a coded signal to modulate the heating source emission is that its time duration and its bandwidth are uncorrelated, *i.e.* the signal duration can be increased while maintaining the bandwidth unaltered [16]. The SNR level can be thus enhanced quite arbitrarily by employing a sufficiently long coded signal.

In addition, both time- and frequency-domain analyses can be performed effectively and contextually through PuCT: the Fourier analysis can be implemented on the acquired raw data while the time-domain analysis is performed on the output of the Pulse-Compression (PuC) procedure, which consists in the application of a proper matched filter over the acquired raw thermogram time series to retrieve an estimate of the impulse response $h(t)$ for each pixel. However, only an estimate $\tilde{h}(t)$ of the $h(t)$ is attained after PuC. This is because the employed coded excitation is both time- and band-limited, so that an inherent mathematical noise is introduced by the procedure.

The mathematical noise introduced by PuC, and hence the quality of the retrieved $\tilde{h}(t)$ in the impulse response estimate, is usually quantified in terms of main-lobe width, *i.e.* range resolution, and side lobes' level, *i.e.* defect detection capability. These quantities strictly depend on (i) the effectiveness of the employed PuC algorithm, (ii) the time–frequency characteristics of the coded signal used and (iii) on the matched filter used for the compression. Concerning (i), Silipigni et al. [15] proposed an optimised strategy to implement the PuC algorithm in PuCT. For point (ii), several references showed the pros and cons arising from the use of linear and non-linear frequency-modulated 'chirp' signals and binary pseudo-noise sequences in PuCT [13,15,17,18]. However, there is still the need to investigate and compare the use of different matched filters (point (iii)) in terms of $\tilde{h}(t)$ quality in combination with linear and non-linear chirp signals.

Despite the use of a baseband linear chirp signal representing the simplest and yet robust frequency-modulated heating stimulus employed in PuCT, it has been shown that employing a tailored signal to deliver energy according to a target power spectrum, *e.g.* a non-linear chirp as in the present case, helps maximising the energy spread at low frequencies, leading to an improved SNR for deeper defects [17,18]. Nevertheless, the $\tilde{h}(t)$ retrieved using a baseband linear chirp is less prone to side lobes with respect to the one obtained employing a bandpass non-linear chirp, thus resulting in a more accurate reconstruction of the ideal $h(t)$. Recently, Burrascano et al. [19,20], pioneered the use of the so-called Reactance Transformation to design an optimal matched filter in PuC applications relying on baseband chirp signals, which promises a significant reduction of the side lobes.

In this paper, a baseband linear chirp and a bandpass non-linear exponential chirp signal were exploited to modulate the emission of LED chips for inspecting a 3D-printed polymethyl methacrylate (PMMA) sample containing 16 flat-bottom holes of different depths. The use of different matched filters was investigated and their performances were qualitatively compared in terms of both $\tilde{h}(t)$ and thermograms' quality, and quantitatively in terms of SNR. It was shown that the combined use of a non-linear

chirp signal with an optimal matched filter obtained from a Reactance Transformation maximised the detection capability of deeper defects while maintaining a high quality of the retrieved $\tilde{h}(t)$, hence higher SNR.

The paper is organised as follows: an introduction on PuC is given in Section 2. Section 2.1. provides details on linear and non-linear chirp signals. Section 2.2. gives an insight on the different matched filters approaches used: Wiener Filter, Hann and Reactance-based window. Section 3 explains the experimental set-up and the SUT. In Section 4, the results will be shown and discussed, and finally in Section 5, the paper will be concluded, and future prospects will be mentioned.

2. Theory of PuC

PuC is a measurement technique employed to estimate the impulse response $h(t)$ of Linear Time Invariant (LTI) systems in poor SNR conditions and it was firstly used in RADAR to improve the range resolution while maintaining the peak power of the transmitted signal relatively low [21]. In standard PT, flash lamps are usually exploited to heat the sample by means of a light pulse significantly shorter than the typical cooling time of the sample itself. Thus, the heating stimulus exciting the LTI system can be modelled as a Dirac's Delta function $\delta(t)$, so that for each pixel, the corresponding impulse response $h(j_x, j_y, t)$ is directly retrieved as the pixel's temperature/emissivity time trend (see Figure1(a)). Useful information about the sample are then obtained by analysing both the heating and the cooling trend of the $\{h(j_x, j_y, t)\}$ within a chosen range of interest T_h.

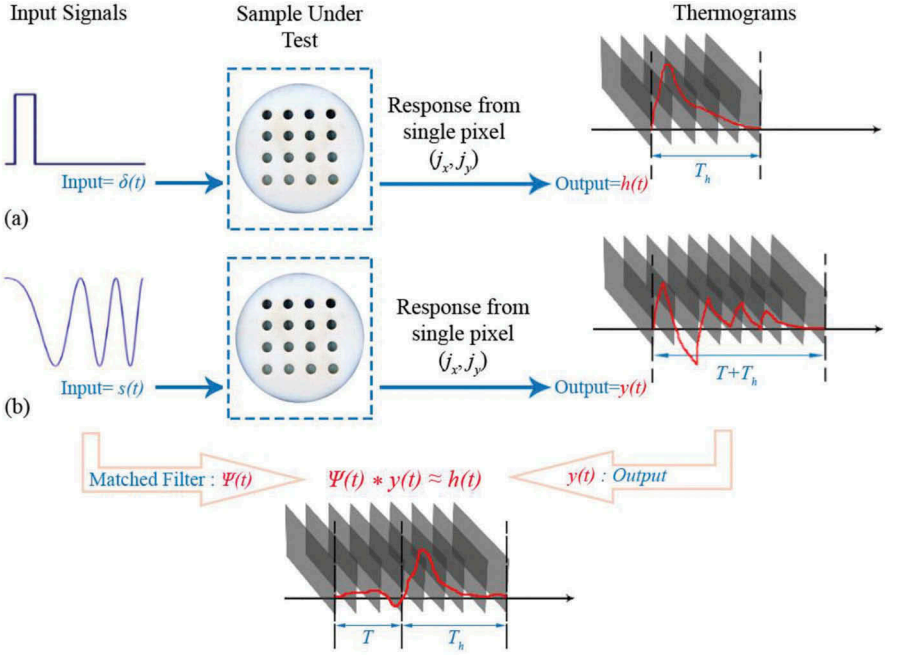

Figure 1. Comparison between (a) Pulsed Thermography (PT) and (b) Pulse-Compression Thermography (PuCT).

On the other hand, PuCT requires further processing steps, as it relies on the existence of two signals $\{s(t), \psi(t)\}$ such that their convolution $\tilde{\delta}(t)$ approximates the Dirac's Delta Function $\delta(t)$:

$$s(t) * \psi(t) = \tilde{\delta}(t) \approx \delta(t) \tag{1}$$

In the previous expression, '$*$' is the convolution operator, $s(t)$ is the input signal of duration T and bandwidth B, $\tilde{\delta}(t)$ is the PuC resolution function and $\psi(t)$ so-called 'Matched' filter. The standard $\psi(t)$ is nothing but the time-reversed replica of $s(t)$. However, in the next sections, we will show that $\psi(t)$ must be modified to optimise the quality of the resolution function and hence the PuCT.

Practically, in a PuC measurement protocol, an estimate of the impulse response $h(t)$ of the LTI system is retrieved by using the coded signal $s(t)$ as input and by applying the $\psi(t)$ on the output signal $y(t)$:

$$\tilde{h}(t) = y(t) * \psi(t) = h(t) * s(t) * \psi(t) \approx h(t) \tag{2}$$

In PuCT, an impulse response $\tilde{h}_{x,y}[n]$ is estimated for each pixel of coordinate (x, y), where $s_{x,y}[n]$ is the pixel intensity/emissivity/temperature at the nth frame, $\{n \in [1, N]\}$. Equation (3) shows the process for a single pixel of the acquired image in the presence of an Additive White Gaussian Noise, shown here by the term $e(t)$, uncorrelated to $\psi(t)$.

$$\begin{aligned} \tilde{h}(t) = y(t) * \psi(t) &= h(t) * \underbrace{s(t) * \psi(t)}_{=\tilde{\delta}(t)} + e(t) * \psi(t) \\ &= h(t) * \tilde{\delta}(t) + \tilde{e}(t) \approx h(t) + \tilde{e}(t) \end{aligned} \tag{3}$$

Figure1 depicts a sketch of the PuCT procedure compared with that of PT: in PT (Figure 1 (a)), the excitation is considered instantaneous and the sample's thermal impulse response is measured for a time T_h, which is the impulse response time duration, *i.e.* the time range of interest of the sample's impulse response from which features of interest can be inferred. In PuCT (Figure 1(b)), the sample is excited with a coded excitation of duration T and thermograms are collected for an overall time duration of $T + T_h$. After the application of the PuC algorithm, an estimated impulse thermal response of duration T_h is retrieved. Note that a step-heating contribution must be removed in order to apply successfully the PuC procedure [15]. Finally, it should be mentioned that the contribution of lateral heat diffusion in general is not negligible, and the same holds here in the PuCT. However, advanced algorithms have been recently proposed to cope with this problem and may be used in the future to further enhance the $\tilde{h}(t)$ reconstruction quality [22].

2.1. Chirp signals

A chirp signal is a frequency-modulated signal whose instantaneous frequency varies linearly or non-linearly within a chosen range. A general mathematical definition of a chirp is given as

$$s(t) = \sin(\phi(t)) \tag{4}$$

with $\phi(t)$ being the instantaneous signal phase [16,23]. The design of a chirp strictly depends on the definition of the instantaneous frequency $f_{ist}(t)$:

$$f_{ist}(t) = \frac{1}{2\pi}\frac{d\phi(t)}{dt} \tag{5}$$

For a linear chirp signal, the phase is a quadratic function $\phi(t) = f_0 t + \frac{B}{2T}t^2$, leading to $f_{ist}(t)$ that is a linear function of time:

$$f_{ist}(t) = f_0 + \frac{B}{T}t \tag{6}$$

where B is the bandwidth $B = f_1 - f_0$, that is the difference between the initial and the final value of the instantaneous chirp frequency. Note that if $f_1 > f_0, B > 0$, then $f_{ist}(t)$ increases as time elapses and the chirp is called 'up' chirp; otherwise if $f_1 < f_0$, then $f_{ist}(t)$ decrease as time elapses and the chirp is a 'down' chirp. The chirp signals employed in this work are 'up'.

When $\phi(t)$ varies neither linearly (*i.e.* a single-tone) nor quadratically, the resulting signal is a non-linear chirp. A non-linear chirp can be defined in two main ways: (i) by starting from the trajectory of its $f_{ist}(t)$ in the desired range $[f_0, f_1]$ and integrating it to retrieve the phase function $\phi(t)$; and (ii) by starting from a target power spectrum following the procedure reported in [23]. In the present case, an exponential cosine non-linear chirp signal was used and designed by following the procedure reported by Novak et al. [24]. Equation (7) gives the analytical expression for the said signal:

$$s(t) = cos\left(2\pi f_0 L\left[e^{\frac{t}{L}} - 1\right]\right) \tag{7}$$

with L being the rate of the exponential increase in frequency that depends on T and the chosen f_1:

$$L = \frac{T}{log_e\left(\frac{f_1}{f_0}\right)} \tag{8}$$

For such signal, the expression of the $f_{ist}(t)$ and $\phi(t)$ is

$$f_{ist}(t) = f_0 e^{\frac{t}{L}} \tag{9}$$

$$\phi(t) = 2\pi f_0 L\left[e^{\frac{t}{L}} - 1\right] \tag{10}$$

Note that Equation (9) clearly shows that an exponential chirp cannot start from $f_0 = 0$, but must be bandpass. Except for this limitation, linear and non-linear chirp signals can be tailored to span over a desired range of frequencies $[f_0, f_1]$. It should be noted that the duration T of the coded excitation sets the overall energy emitted towards the sample by the heating source, whilst the correct choice of f_0 and f_1 establishes and yet limits the maximum penetration depth within the SUT. Moreover, f_0 and f_1 must be chosen to guarantee a sufficiently high $T \times B$ product to achieve a good approximation of the $\tilde{h}(t)$ [19,20]. Further, the $T \times B$ product can be optimised for a given inspection using chirp excitations, as these class of signals shows completely uncorrelated B and T.

For these reasons, $f_0 = 0$ Hz, $f_1 = 1$ Hz and T = 80.0 s were chosen for the baseband linear chirp signal while the following values were selected for the exponential non-

linear chirp: $f_0 = 0.01$ Hz, $f_1 = 1$ Hz and T = 80.8 s. Please note that a special phase alignment condition was also considered for the employed exponential chirp; thus, the effective time duration slightly differs with respect to the linear chirp one [24]. The two employed signals are depicted in Figure 2.

For a linear up-chirp, the instantaneous frequency slope is constant with time. On the other hand, the non-linear chirp instantaneous frequency is skewed towards the low frequency range; thus, it can improve the defect detection capabilities for deeper defects since most of the delivered energy is at low frequencies. Nevertheless, baseband linear chirps exhibit in general lower side lobe levels after PuC process than bandpass non-linear ones. Thus, a proper matched filter must be designed to reduce the side lobe levels in non-linear chirp while improving the probing depth. The approaches used here to reduce the side lobes are reported and described in the next section.

2.2. Problem of side lobes and strategies to reduce them

The PuC's resolution depends on both $s(t)$ and $\psi(t)$. Since they are time–frequency-limited signals, the resulting $\tilde{\delta}(t)$ is always an approximation of the ideal $\delta(t)$ and it is characterised by a main lobe of finite amplitude and width and by side lobes of decreasing amplitude.

In general, the use of a matched filter $\psi(t)$ defined as time-reversal replica of $s(t)$ makes the spectrum of $\tilde{\delta}(t)$ to be real, since the phase of $\psi(t)$ maximises the PuC output SNR at a specific time instant at which $s(t)$ is found possibly buried in noise in the acquired $y(t)$. The application of the matched filter over the recorded thermogram series, performs a spectral phase correspondence. This in turn produces the desired PuC output peak at a given time instant, and a spectral amplitude with maximised SNR at the said peak position. It can be shown that once the phase matching of $\psi(t)$ and $s(t)$ is assured, the filter response amplitude $|\Psi(f)|$ can be shaped to a specific aim, for instance to maximise the range resolution by using windows or to maximise the SNR of the retrieved PuC output. For the latter, it can be demonstrated that employing $\psi(t) = s(-t)$ maximises the SNR obtained after PuC. On the other hand, the so-

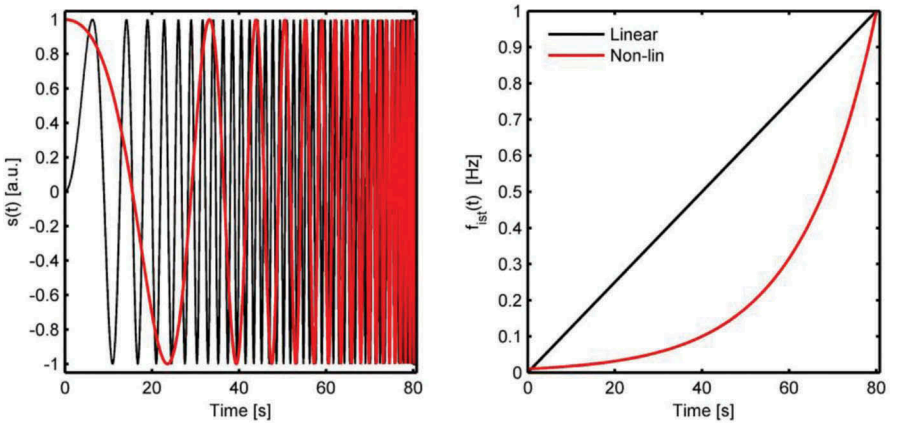

Figure 2. Plots of linear and non-linear chirp. Left: Linear (black) and non-linear (red) chirp signals, Right: $f_{ist}(t)$ versus time for the same signals.

obtained $\tilde{\delta}(t)$ shows a high level of side lobes, which hampers the faithful reconstruction of the thermal response of the SUT. Reduction in side lobe levels can be realised by means of (i) different windowing functions $a(t)$ on the matched filter, such that $\psi(t) = a(t)s(-t)$ [16,25], or (ii) by exploiting a Wiener filter approach to design an optimal $\psi_W(t)$ [15].

Regarding approach (i), the window function can significantly reduce side lobes level at the cost of widening the main lobe. A low-pass Hann and a Reactance-based window have been applied here on the linear and non-linear chirp, respectively. Please note that the Reactance-based window is applied only on the exponential non-linear chirp for its passband characteristic. The reader is referred to Refs [19,20] for further details.

Concerning (ii), a possible method of decreasing the sensitivity of the PuC output to noise is to bound the frequency response of the matched filter $\Psi(f)$ according to a specific frequency selection rule. To this aim, the Wiener filter approach is used here to design an optimal $\psi_W(t)$, which is described in frequency as in Equation (11):

$$\psi_W(t) = IFFT\left(\frac{\Psi(f)}{|\Psi(f)|^2 + a + b \cdot |f|}\right), \tag{11}$$

where IFFT stands for Inverse Fast Fourier Transform operator. a and b are two regularisation parameters, the former regulating the filter effect over the entire bandwidth, the latter penalising the high frequencies. The employed value for the regularisation parameters in this case was $a = b = 0.1$. Equation (11) shows that the $\psi_W(t)$ has the same phase profile of the $\psi(t)$ but with modified spectrum amplitude so as to emphasise the frequency band in which the frequency spectrum of the $s(t)$ is known to be higher.

3. Experimental set-up and SUT

A National Instrument PCI-6711 Arbitrary Waveform Generator (AWG) board and a National Instrument 1433 Camera Link Frame Grabber were connected to a PC, and an ad hoc virtual instrument developed in LabVIEW managed the signal generation/acquisition. The AWG board provided both the wanted linear chirp excitation and a reference clock signal (CLK) for triggering the IR camera acquisition, which was a Xenics Onca-MWIR-InSb camera placed in reflection mode. A sketch of the experimental set-up used is depicted in Figure 3. The coded signal was input into a TDK Lambda GEN 750W power supply that fed eight LED chips in the visible spectrum placed at about 30 cm from the SUT. The LED chips are capable to provide a maximum overall power of 400 W. The thermograms were acquired at 40 FPS.

The SUT was a synthesised PMMA specimen realised by additive manufacturing. The sample contains 16 flat-bottom holes of 10 mm radius and various depths. A sketch of the sample is depicted in Figure 4. The thermal diffusivity of the sample was directly measured by averaging three readings from an *Applied Precision* ISOMET-2104. For this purpose, a PMMA sound sample, *i.e.* without any defects and having the same dimensions of the SUT, was realised using the same additive manufacturing procedure. The thermal diffusivity was measured as 0.108 m^2/s. As PMMA is partially translucent within the visible spectrum, the SUT was painted by black paint on the inspection surface. All measurements have been carried out on the defect-free surface, as depicted in Figure 4 (inspection side).

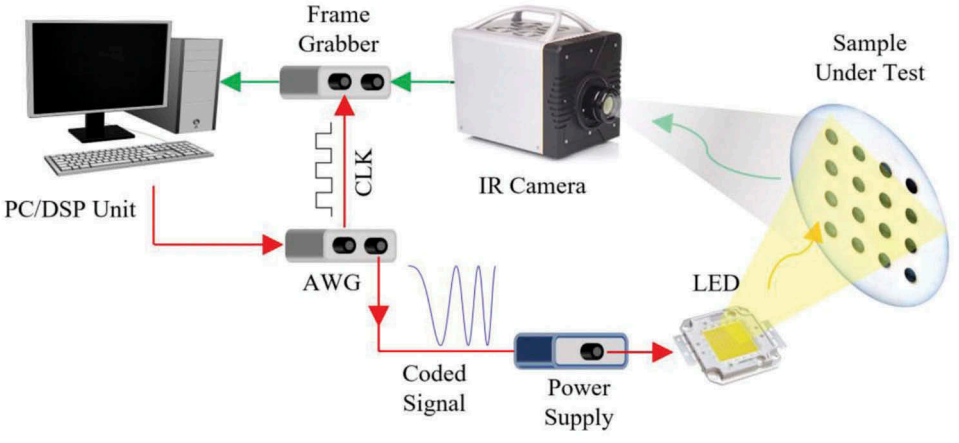

Figure 3. Sketch of the experimental set-up.

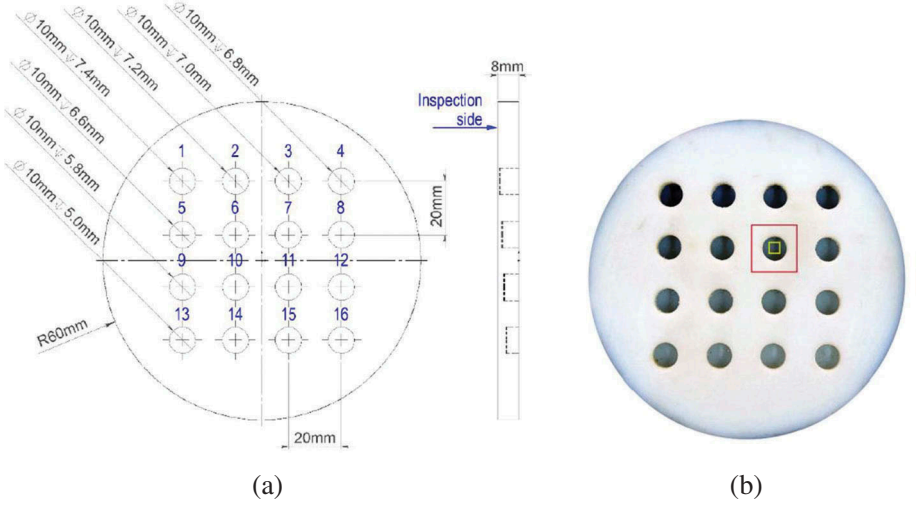

Figure 4. Sketch of the SUT (a) detailed drawing of the SUT containing 16 flat-bottom holes with depths starting from 7.4 mm depth with steps of 0.2 mm. The defects have been numbered to be better distinguished. (b) The real image of the SUT and the defected (yellow marker) and reference (red marker) areas used for the SNR definition.

4. Results and discussion

To compare the efficiency of the various strategies, the normalised impulse response of the SUT in a certain point, *i.e.* onto the seventh artificial defect location, has been graphed. The impulse response was obtained using linear and non-linear chirp signals. For both linear and non-linear chirp, three cases were investigated: (i) without any windowing function and only using standard matched filter, (ii) by using Wiener filter instead of the standard matched filter, and (iii) with standard matched filter in combination with a window function. In the linear chirp case, a low-pass Hann window was used, while in the case of non-linear chirp, the same Hann window was firstly modified by means of the

reactance transformation introduced in [19,20] and then applied to the matched filter. Figure 5 depicts the graphs of the various impulse response trends obtained.

Side lobes are visible for the impulse response obtained without using any filter or window. As expected, the use of the Wiener filter and the windowing functions reduced side lobes, but at the cost of wider main lobe. For a quantitative comparison between the results and the validation of each strategy, the SNR value in time has been used as the figure of merit as follows:

$$SNR_k(t) = \frac{h_k(t) - \bar{h}(t)}{\sigma_h(t)}, \tag{12}$$

where $h_k(t)$ is the impulse response of the kth defect averaged over the region shown in Figure 4(b) by the yellow box, $\bar{h}(t)$ is the impulse response averaged over the area shown in Figure 4(b) by the red box and $\sigma_h(t)$ is its standard deviation over the same area.

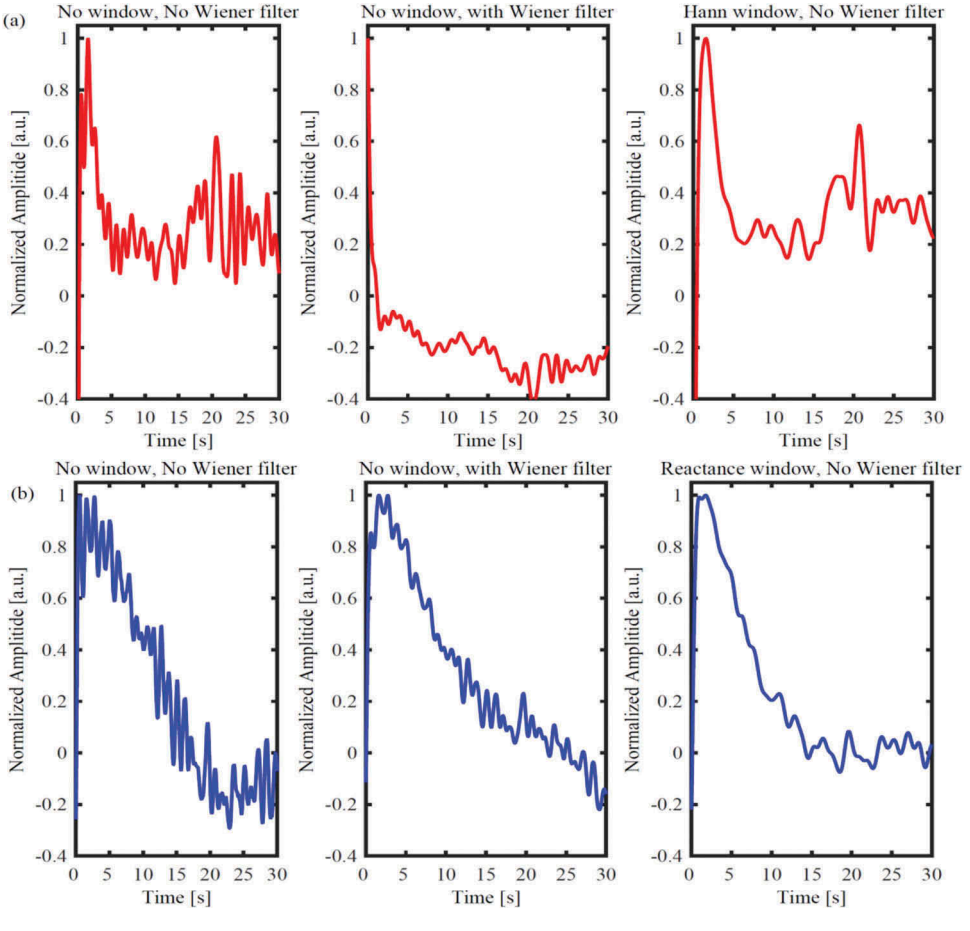

Figure 5. Comparison of the impulse responses obtained on the PMMA sample on defect number 7 by (a) linear chirp, (b) non-linear chirp. Results are depicted for the impulse response direct from PuC process (standards matched filter) without windowing and in combination with Wiener filter and windowing functions.

Figure 6 depicts the maximum SNR values obtained for each proposed strategy for Defect 7, which represents the deepest straightforward-visible defect with the exploited set-up. The SNR values are significantly improved by exploiting the exponential non-linear chirp with respect to linear chirp. The non-linear chirp in combination with reactance window exhibits the best result. In case of the linear chirp, application of Wiener filter and the Hann window provides almost similar results in terms of SNR.

After the calculation of the maximum SNR values for each strategy, the thermograms corresponding to the maximum value in time for each proposed strategy were found and depicted in Figure 7, in which the thermograms in the first row correspond to non-

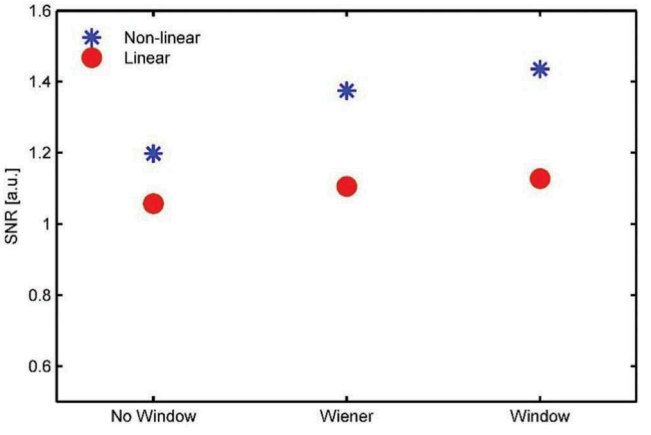

Figure 6. Maximum SNR values for different applied strategies on linear and non-linear chirp signals at Defect 7 location.

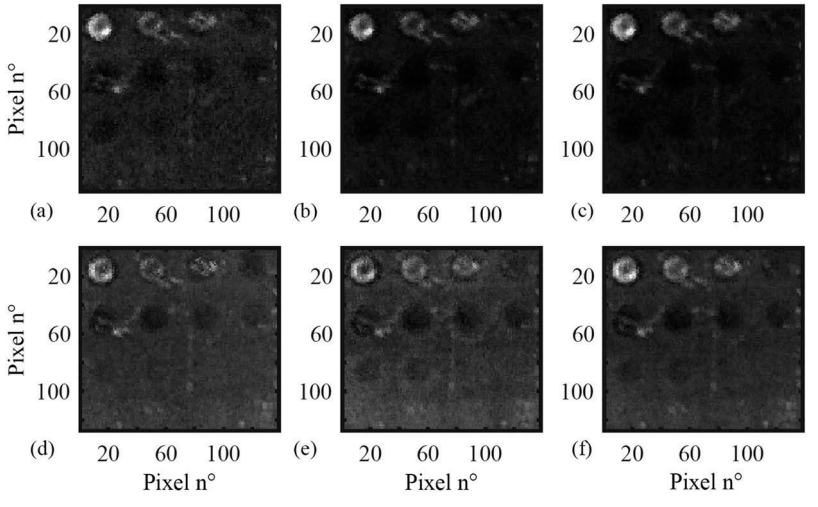

Figure 7. Thermograms acquired at the peak of SNR values for Defect 7 location for each strategy. (a) to (c) respectively: exponential non-linear chirp without window and Wiener, with Wiener filter and without window, without Wiener and with reactance window, (d)–(f), respectively: linear chirp without window and Wiener, with Wiener filter and without window, without Wiener and with Hann window.

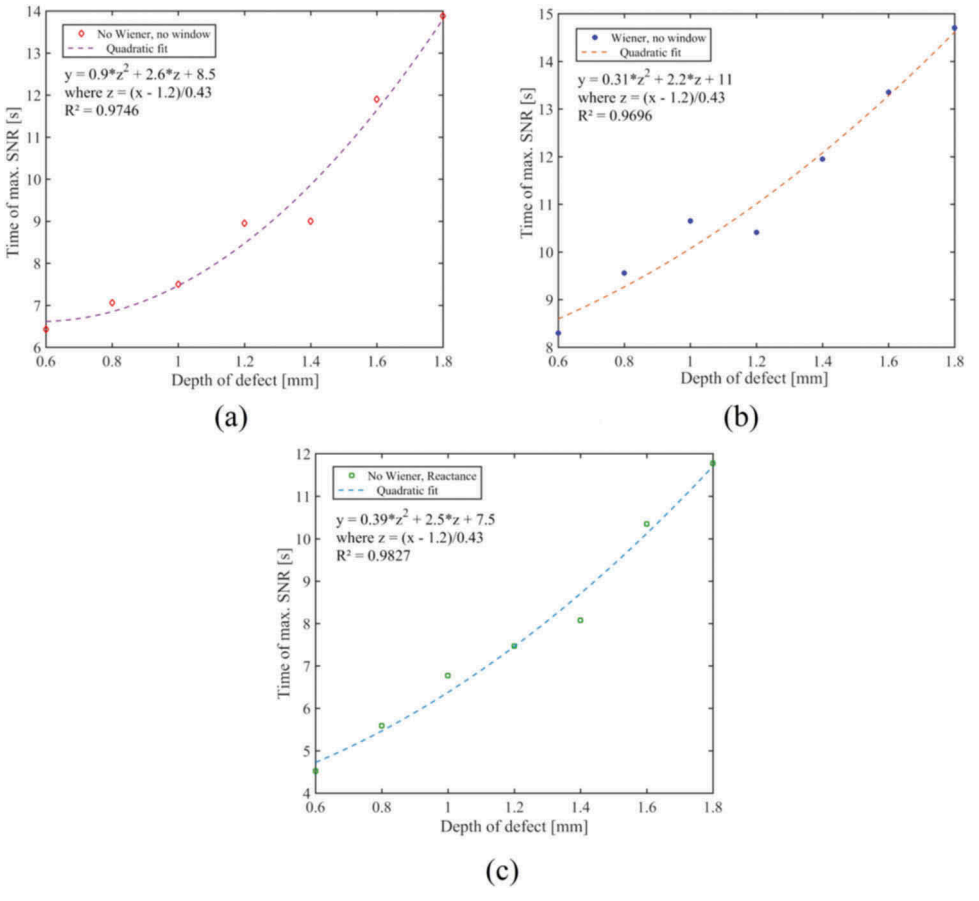

Figure 8. Relation between the time instant at which the maximum SNR values versus defect's depth for different strategies, along with the fitting data showing the quadratic relation between the time of maximum SNR and the depth for the case of non-linear chirp (a) No Wiener, no window, (b) Wiener, no window, (c) No Wiener, Reactance.

linear chirp and the second-row shows the linear chirp results. One can see that the outcome of the exponential non-linear chirp is clearer, and deeper defects are visible (third row of defects is visible) with higher contrast, which is in a good agreement with quantitative results.

Figure 8 shows another quantitative evaluation of the results by plotting the time instant at which the maximum SNR values occur for each strategy versus the defect's depth, in this case only for non-linear chirp. The fitted curve shows a quadratic relation between these two values as expected [15,26].

5. Conclusion and future work

The use of a non-linear exponential frequency-modulated chirp signal in combination with a proper window improved the defect detection capability of deeper defects in a PuCT experiment implemented on a 3D-printed PMMA sample with

artificial defects. The proposed approach can be easily extended to any frequency-modulated PuCT scheme, where defects can occur in a quite wide range of depths requiring a broad range of excitation frequencies. Similarly, the proposed procedure is still valid when sinusoidal chirps are replaced by squared frequency-modulated signals. In conclusion, by combining long excitations typical of LT, and time-domain analysis of PT, the defect detection capability of the proposed PuC procedure can outperform that of those conventional techniques. Moreover, the reduction of the PuC side lobes provides a quite good quality of the reconstruction of the pixels' impulse responses. Therefore, PuCT can also be a potential alternative to PT even if the use of advanced post-processing procedures specific of thermography, such as TSR or partial least squares-based algorithms, are desired. As a future development, the exponential-chirp-based PuCT procedure that has been proposed here can be fully exploited by implementing also the analysis of possible non-linear phenomena, thanks to the special characteristics of the exponential chirp signals [24].

Disclosure statement

No potential conflict of interest was reported by the authors.

Funding

This research work has been partially supported from the European Union's Horizon 2020 research and innovation programme under the Marie Skłodowska–Curie grant agreement No. 722134 – NDTonAIR.

Notes on contributors

Hamed Malekmohammadi received his B.Sc. in mechanical engineering from K.N. Toosi UNiversity of Technology, Tehran-Iran and his M.Sc. degree in NDT from Dresden International University, Germany. He is now with the department of Engineering, University of Perugia as the Ph.D. fellow and researcher involved in "NDTonAIR" Marie Skłodowska-Curie European H2020 project. His main field of interest is non-destructive testing and evaluation techniques, especially electromagnetic techniques and thermography. He has gained more than 14 years of experience with industrial manufacturing and NDT applications.

Stefano Laureti received the B.Sc. degree in energy engineering and the M.Sc. degree (cum laude) in industrial engineering from the University of Perugia, Italy, in 2011 and 2013 respectively, and the co-tutelle Ph.D. degree in engineering jointly from the School of Engineering, University of Warwick, U.K., and the University of Perugia in 2017. He is currently a post-doctoral Researcher and the Project Manager of the Marie Skłodowska-Curie European H2020 training network "NDTonAIR", with the University of Perugia. His research interests include acoustic metamaterials, phononic crystals, thermography, ultrasonic testing, eddy current testing, image processing, and pulse-compression, in which fields he authored and co-authored more than 40 journal papers, book chapters and conference proceedings.

Pietro Burrascano worked at the headquarters of Telespazio SpA from 1981 to 1983 and was involved in satellite telecommunications systems planning. In 1984 he joined the Department Info-Com at University of Rome "Sapienza" as a researcher. Since 1994 is a full professor of Electrical Engineering at the University of Perugia. He has been the coordinator of a number of national and international applied research projects and the author of more that 100 scientific indexed papers

and book chapters in the fields of signal and image processing and non-destructive testing and evaluation.

Marco Ricci received his Laurea degree and the PhD from the University of Rome "Sapienza" in 2002 and 2006 respectively. From 2007 to 2016 he was with the Department of Engineering of the University of Perugia as Assistant Professor. From 2016 he is Associate Professor of Electrical Engineering at the University of Calabria. He is the author of more than 90 publications including international journals, conference proceedings and book chapters in the fields of non-destructive testing and evaluation, signal and image processing, spintronics and quantum information.

ORCID

H. Malekmohammadi http://orcid.org/0000-0002-8042-2339

References

[1] Maldague X. Nondestructive evaluation of materials by infrared thermography. London: Springer; 1993.
[2] Meola C, Carlomagno GM, Giorleo L. The use of infrared thermography for materials characterization. J Mater Process Technol. 2004;155:1132–1137.
[3] Maldague X. Theory and practice of infrared thermography for nondestructive testing. New York: Wiley series in microwave and optical engineering. Wiley; 2001.
[4] Sfarra S, Ibarra-Castanedo C, Paoletti D, et al. Infrared vision inspection of cultural heritage objects from the city of l'Aquila, Italy and its surroundings. Mater Eval. 2013;71(5):561–570.
[5] Laureti S, Sfarra S, Malekmohammadi H, et al. The use of pulse-compression thermography for detecting defects in paintings. NDT E Int. 2018;98:147–154.
[6] Senni L, Ricci M, Palazzi A, et al. On-line automatic detection of foreign bodies in biscuits by infrared thermography and image processing. J Food Eng. 2014;128:146–156.
[7] Yi Q, G Y T, Malekmohammadi H, et al. New features for delamination depth evaluation in carbon fiber reinforced plastic materials using eddy current pulse-compression thermography. NDT E Int. 2019;102:264–273.
[8] Shepard SM. Advances in pulsed thermography. In Rozlosnik AE, Dinwiddie RB, editors: Thermosense XXIII, International Society for Optics and Photonics. Orlando, Florida: Aerospace/Defense Sensing, Simulation, and Controls; Vol. 4360; 2001 Mar. p. 511–516. https://doi.org/10.1117/12.421032
[9] Ibarra-Castanedo C, Bendada A, Maldague X. Image and signal processing techniques in pulsed thermography. GESTS Int Trans Com Sci Eng. 2005;22(1):89–100.
[10] Tuli S, Mulaveesala R. Defect detection by pulse compression in frequency modulated thermal wave imaging. Quant Infrared Thermogr J. 2005;2(1):41–54.
[11] Mulaveesala R, Tuli S. Digitized frequency modulated thermal wave imaging for nondestructive testing. Mater Eval. 2005;63(10):1046–1050.
[12] Tabatabaei N, Mandelis A. Thermal-wave radar: a novel subsurface i maging modality with extended depth-resolution dynamic range. Rev Sci Inst. 2009;80(3):034902.
[13] Mulaveesala R, Ghali VS. Coded excitation for infrared non-destructive testing of carbon fiber reinforced plastics. Rev Sci Inst. 2011;82(5):054902.
[14] Gong J, Liu J, Qin L, et al. Investigation of carbon fiber reinforced polymer (CFRP) sheet with subsurface defects inspection using thermal-wave radar imaging (TWRI) based on the multi-transform technique. NDT E Int. 2014;62:130–136.
[15] Silipigni G, Burrascano P, Hutchins DA, et al. Optimization of the pulse compression technique applied to the infrared thermography nondestructive evaluation. NDT E Int. 2017;87:100–110.
[16] Hutchins D, Burrascano P, Davis L, et al. Coded waveforms for optimised air-coupled ultrasonic nondestructive evaluation. Ultrasonics. 2014;54:1745–1759.

[17] Dua G, Mulaveesala R, Siddique JA. Effect of spectral shaping on defect detection in frequency modulated thermal wave imaging. J Opt. 2015;17(2):025604.
[18] Laureti S, Silipigni G, Senni L, et al. Comparative study between linear and non-linear frequency-modulated pulse-compression thermography. Appl Opt. 2018;57(18):D32–D39.
[19] Burrascano P, Laureti S, Ricci M, et al. Reactance transformation to improve range resolution in pulse-compression detection systems. 40th International Conference on In Telecom. and Signal Proc. (TSP); 2017 July 5–7; Barcelona, Spain: IEEE. p. 480–483.
[20] Burrascano P, Laureti S, Senni L, et al. Pulse compression in nondestructive testing applications: reduction of near sidelobes exploiting reactance transformation. IEEE Trans Circuits Syst I: Reg Papers. 2018;99:1–11.
[21] Klauder JR, Price AC, Darlington S, et al. The theory and design of chirp radars. Bell Labs Tech J. 1960;39(4):745–808.
[22] Burgholzer P, Thor M, Gruber J, et al. Three-dimensional thermographic imaging using a virtual wave concept. J Appl Phys. 2017;121(10):105102.
[23] Pollakowski M, Helmut E. Chirp signal matching and signal power optimization in pulse-echo mode ultrasonic nondestructive testing. IEEE Trans Ultrason Ferroelectr Freq Control. 1994;41(5):655–659.
[24] Novak A, Simon L, Kadlec F, et al. Nonlinear system identification using exponential swept-sine signal. IEEE Trans Instrum Meas. 2010;59(8):2220–2229.
[25] Pallav P, Gan TH, Hutchins DA. Elliptical-Tukey chirp signal for high-resolution air-coupled ultrasonic imaging. IEEE Trans Ultrason Ferroelectr Freq Control. 2007;54(8):1530–1540.
[26] Lopez F, De Paulo Nicolau V, Ibarra-Castanedo C, et al. Thermal-numerical model and computational simulation of pulsed thermography inspection of carbon fiber-reinforced composites. Int J Therm Sci. 2014;86:325–340.